Numerical Study of Natural Convection of Nanofluids in an Inclined Flat Bottom Flask Using Finite-Volume Approach

Chafai, Nadjib*+

Laboratory of Electrochemistry of Molecular Materials and Complex (LEMMC). Department of Process Engineering, Faculty of Technology, University of Ferhat ABBAS Setif-1, El-Mabouda campus, 19000 Sétif, ALGERIA

Salhi, Hicham

Laboratory of Applied Research in Hydraulics, University of Mustapha Ben Boulaid-Batna 2,Batna, ALGERIA

Benobouguerra, Khalissa•; Chafaa, Salah

Laboratory of Electrochemistry of Molecular Materials and Complex (LEMMC). Department of Process Engineering, Faculty of Technology, University of Ferhat ABBAS Setif-1, El-Mabouda campus, 19000 Sétif, ALGERIA

ABSTRACT: *In this work, we study numerically the natural convection of NanoFluids (NF) in an inclined flat bottom flask; it is one of the laboratory flasks used in organic chemistry synthesis. The main reason for this study is to enhance the thermal properties of the reaction medium inside the flat bottom flask and to ameliorate the rate of chemical reactions using nanofluids. The flat bottom wall is maintained at a constant high-temperature T_h. While the top, left and right walls of the cavity are maintained at a low-temperature T_L. The NF comprises Cu and Al_2O_3 NanoParticles (NP) suspended in pure water. The governing equations are solved numerically using the finite-volume approach and formulated using the Boussinesq approximation. In this simulation we examined the effects of the NP volume fraction (φ) from 0% to 5%, the Rayleigh number from 10^3 to 10^6, the various inclination angles of enclosure (γ=0°,5°,10°, 15°) and the NF type (Cu and Al_2O_3) on the flow streamlines, isotherm distribution, and Nusselt number. The obtained results show that the addition of Cu and Al_2O_3 NP increases the mean Nusselt number which enhances the heat transfer in the flat bottom flask and causes significant changes in the flow pattern. In addition, the mean Nusselt number is increased with increasing the Rayleigh number and the volume fraction, and the best results have been obtained from the Cu nanofluid. Also, as the inclination angle increases the mean Nusselt number decreases, and the highest value of the Nusselt number was obtained for a vertical enclosure (γ=0°). The obtained streamlines are mostly symmetric and their values are generally increased by increasing the Rayleigh number and volume fractions of NPs. Besides, the obtained isotherms generally follow the geometry of the flat bottom flask.*

KEYWORDS: *Natural convection; Nanofluids; Flat bottom flask; Numerical study; Heat transfer enhancement.*

INTRODUCTION

The use of heat transfer fluids has great importance in the petrochemical and chemical industries, especially, their applications in heating and cooling systems. The natural convection heat transfer in partially heated cavities is an important phenomenon in many practical and industrial applications, such as industrial cooling installations or large-scale heat exchangers (used in chemical processing plants). In general, laboratory flasks used in organic chemistry synthesis and analytical chemistry have an extensive range of applications such as heating, boiling, and evaporation. The study of the natural convection heat transfer of nanofluids in this type of flask is original and has not been conducted previously. So, the difference between this study and other published papers is the geometry of the cavity, which is new and interesting. For most chemical reactions, the reaction rate increases by increasing temperature. So, it is always useful to work at optimum temperature. As well as, the use of the catalysts increases the reaction rate. Generally, Cu and Al_2O_3 are used as catalysts for certain chemical reactions. So adding Cu and Al_2O_3 particles in the reaction medium and increasing the temperature will increase the reaction rate. The use of nanoparticles enhances the thermal properties for heat transfer and heat storage of the reaction medium inside the flat bottom flask, and also enhances the rate of chemical reactions (the thermal activation of chemical reactions).

During the last two decades, nanofluids are becoming a new pivotal component of heat transfer liquid and are envisioned to describe a fluid in which nanometer-sized particles are suspended in conventional heat transfer basic fluid [1-4]. They have been developed, used, and studied extensively by many researchers [5-8]. *Aminossadati* and *Ghasemi* [9] studied the natural convection heat transfer in an enclosure filled with NF. Their results showed that higher cooling performance can be achieved by adding NPs into pure water. By drawing on a two-dimensional numerical simulation of the natural convection of NF in a vertical rectangular enclosure, *Khanafer et al.* [10] found that the heat transfer across the enclosure increases with the volumetric fraction of the copper NPs in water at any given Grash of number. *Hwang et al.* [11] studied free convection using a rectangular cavity heated from below (Bénard convection) with NF. Also, *Hatami et al.* [12] investigated the natural convection heat transfer of nanofluids in a circular-wavy cavity and demonstrate that the shape of the wavy wall has a significant effect on heat transfer.

Recently, hybrid nanofluids are a new class of fluids that demonstrate excellent heat transfer performance compared to conventional fluids [13-16]. *Chamkha et al.* [17] studied the MHD convection of an Al_2O_3–Cu/Water hybrid nanofluid in an inclined porous cavity with Internal Heat generation/absorption. The impact of volume fraction, Rayleigh number, heat generation, and heat source length and location on magneto-free convective with entropy has been analyzed. The results indicated that the high volume fraction diminishes the thermal performance. Also, the addition of nanoparticles for several Rayleigh numbers causes the thermal performance to be declined.

The inclination angle has a significant impact on the flow and temperature fields and the heat transfer performance at high Rayleigh numbers. *Saury et al.* [18] investigate experimentally the effect of the angle of inclination on the natural convection unsteadiness occurring in an air-filled cavity having two opposite walls respectively heated and cooled at a constant and uniform temperature. *Alinia et al.* [19] performed and analyzed numerically a mixed convection flow of SiO_2–water NF in an inclined enclosed square cavity using a two-phase mixture model to evaluate the influence of control parameters on the heat transfer characteristics of NF.

Geometrical patterns of the cavity can be useful in improving heat transfer performance. The problem of natural convection in a cavity with wavy walls has several engineering applications such as solar collectors, heat exchanger design, electric machinery, and so forth. *Tang et al.* [20] proposed a new 2D quarter-circular enclosure with two sinusoidal wavy walls and two straight walls. As well, the natural convection heat transfer in the investigated cavities containing various types of nanofluids was studied and the effect of the external wavy wall shape was studied by a combined Finite Volume Method (FVM) and Response Surface Method (RSM) method.

Ching-Chang et al. [21] performed a numerical investigation into the natural convection heat transfer characteristics within an enclosed cavity filled with nanofluid. The left and right walls of the studied cavity have a complex-wavy geometry and are maintained at high and low temperatures, respectively. Meanwhile, the upper and lower walls of the cavity are both flat and insulated. The nanofluid comprises Al_2O_3 nanoparticles suspended in pure water. Also, *Ching-Chang et al.* [22] performed a numerical investigation into the natural

convection heat transfer characteristics and entropy generation of water-based nanofluids in an enclosure bounded by wavy vertical walls and flat upper and lower surfaces. Recently, *Ching-Chang et al.* [23] studied the use of the headline technique to estimate the natural convection heat transfer characteristics in an inclined wavy-wall cavity filled with Al_2O_3-water nanofluid.

Salhi et al. [24] carried out a numerical investigation of the natural convection heat transfer performance of a wavy-wall enclosed cavity filled with Ag or TiO_2–water NFs. They reported that the effect of inclination angle and type of temperature is more pronounced at higher Rayleigh numbers. Moreover, it was shown that the heat transfer performance can be optimized by tuning the wavy-surface geometry parameters.

Kashani et al. [25] studied numerically the effects of density inversion of water as well as different wavy patterns on entropy generation and natural convection heat transfer in a two-dimensional cavity filled with the nanoparticle-water mixture. *Sakanova et al.* [26] examined the 3D heat transfer of wavy MCHS and compared it with a rectangular MicroChannel Heat Sink (MCHS). The effect of water and NFs as a coolant in both types of MCHS was discussed. Also, the influence of the wave amplitude, wavelength, flow rate, and volume concentration of three types of NFs on the heat transfer, pressure drop, friction factor, and thermal resistance are discussed and compared with rectangular MCHS. The influences of solar radiation on the two-dimensional stagnation-point flow of nanofluid over a stretching sheet have been investigated by *Ghasemi et al.* [27].

The use of flat bottom flask has gained importance in organic synthesis due to several advantages such as operational simplicity, low cost, and ease of isolation after completion of the reaction. The study of natural convection heat transfer in flasks used in organic chemistry synthesis has great importance in the study of chemical reaction processes and mechanisms.

In our work we studied numerically the natural convection of NF in an inclined flat bottom flask; it is one of the laboratory flasks used in organic chemistry synthesis. The flat bottom wall is maintained at a constant high-temperature T_h. The top left and right walls of the cavity are maintained at a low-temperature T_L. The NF comprises Cu and Al_2O_3 NPs suspended in pure water. The governing equations are solved numerically using the finite-volume

approach and formulated using the commercial software package called Fluent 6.3.26 developed by ANSYS, Inc. We examined the effects of the NP volume fraction (φ) from 0% to 5%, the Rayleigh number from 10^3 to 10^6, the various inclination angles of enclosure ($\gamma=0°,5°,10°, 15°$), and the NF type (Cu and Al_2O_3) on the flow streamlines, isotherm distribution, and average Nusselt number.

THEORETICAL SECTION
Mathematical Formulation
Fig. 1 illustrates the flat bottom flask cavity considered in the present study. As shown, the left and right walls have straight and circular surfaces, while the top and bottom walls are straight. In addition, the cavity has a height H = 6 cm, diameters D = 4 cm, d_1= 1 cm and d_2 = 2 cm, and flask neck L = 2.5 cm. The gravitational force is assumed to act in the negative y-direction.

The mathematical equations describing the physical model are based on the following assumptions: (I) the thermophysical properties are constant except for the density in the buoyancy force (Boussinesq's hypothesis), (II) the base fluid and NPs are in a thermal equilibrium state, (III) the NPs have a uniform size and shape and are well dispersed within the base fluid, (IV) the NF in the cavity is Newtonian, incompressible, and laminar, (V) the radiation heat transfer between the sides of the cavity is negligible when compared with the other mode of heat transfer, and (VI) the process is not dependent on the time (steady state) and the nanofluid flow is stationary and two-dimensional.

In addition, the related mathematical formulations and numerical solution procedures are described below.

Vorticity [20]:

$$\frac{\partial}{\partial x}\left(\omega\frac{\partial \psi}{\partial y}\right) - \frac{\partial}{\partial y}\left(\omega\frac{\partial \psi}{\partial x}\right) = \frac{\mu_{nf}}{\rho_{nf}}\left(\frac{\partial^2 \omega}{\partial x^2} + \frac{\partial^2 \omega}{\partial y^2}\right) + \tag{1}$$

$$\frac{\beta_{nf}}{\rho_{nf}}g\left(\cos(\gamma)\frac{\partial T}{\partial x} - \sin(\gamma)\frac{\partial T}{\partial y}\right)$$

Energy [20]:

$$\frac{\partial}{\partial x}\left(T\frac{\partial \psi}{\partial y}\right) - \frac{\partial}{\partial y}\left(T\frac{\partial \psi}{\partial x}\right) = \tag{2}$$

$$\frac{\partial}{\partial x}\left(\alpha_{nf}\frac{\partial T}{\partial x}\right) + \frac{\partial}{\partial y}\left(\alpha_{nf}\frac{\partial T}{\partial y}\right)$$

Kinematic [20, 24]:

The effective thermal conductivity of the NF is approximated by the Maxwell–Garnetts model [6]:

$$\frac{k_{nf}}{k_f} = \frac{k_s + 2k_f - 2\varphi(k_f - k_s)}{k_s + 2k_f + \varphi(k_f - k_s)} \tag{8}$$

The effective viscosity of a fluid containing a dilute suspension of small rigid spherical particles is given by *Brinkman* [28] as:

$$\mu_{nf} = \frac{\mu_f}{(1 - \varphi)^{2.5}} \tag{9}$$

The radial and tangential velocities are given by the following relations respectively [20, 24]:

$$u = \frac{\partial \psi}{\partial y} \quad ; \quad v = -\frac{\partial \psi}{\partial x} \tag{10}$$

The following dimensionless groups are introduced [20, 24]:

$$X = \frac{x}{H}; \; Y = \frac{y}{H}; \; \Omega = \frac{\omega H^2}{\alpha_f}; \; \Psi = \frac{\psi}{\alpha_f}; \; V = \frac{vH}{\alpha_f}; \; U = \frac{uH}{\alpha_f};$$

$$\theta = \frac{T - T_L}{T_H - T_L}$$

$$\mu_{nf} \frac{\partial}{\partial X}\left(\Omega \frac{\partial \Psi}{\partial Y}\right) - \frac{\partial}{\partial Y}\left(\Omega \frac{\partial \Psi}{\partial X}\right) = \tag{11}$$

$$\left[\frac{Pr}{(1-\varphi)^{2.5}\left((1-\varphi) + \varphi\frac{\rho_s}{\rho_f}\right)}\right]\left(\frac{\partial^2 \Omega}{\partial X^2} + \frac{\partial^2 \Omega}{\partial Y^2}\right) +$$

$$Ra * Pr \left[\frac{1}{\frac{(1-\varphi)\rho_f}{\varphi \rho_s}+1}\frac{\beta_s}{\beta_f} + \frac{1}{\frac{\varphi}{(1-\varphi)}\frac{\rho_f}{\rho_s}+1}\right]\left[\left(\cos(\gamma)\frac{\partial \theta}{\partial x} - \sin(\gamma)\frac{\partial \theta}{\partial y}\right)\right]$$

$$\frac{\partial}{\partial X}\left(\theta\frac{\partial \Psi}{\partial Y}\right) - \frac{\partial}{\partial Y}\left(\theta\frac{\partial \Psi}{\partial X}\right) = \tag{12}$$

$$\frac{\partial}{\partial X}\left(\lambda\frac{\partial \theta}{\partial X}\right) + \frac{\partial}{\partial Y}\left(\lambda\frac{\partial \theta}{\partial Y}\right)$$

$$\frac{\partial^2 \Psi}{\partial X^2} + \frac{\partial^2 \Psi}{\partial Y^2} = -\Omega \tag{13}$$
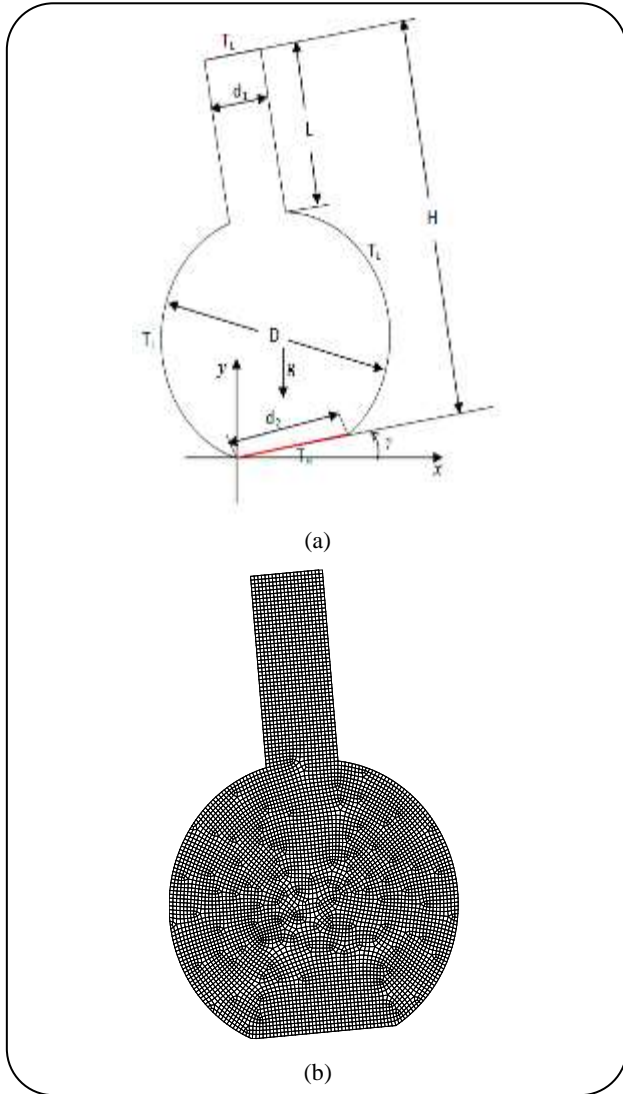
Where:

Fig. 1: Schematic illustration of flat bottom flask enclosed cavity (a) and numerical grid (b).

$$\frac{\partial^2 \psi}{\partial x^2} + \frac{\partial^2 \psi}{\partial y^2} = -\omega \tag{3}$$

$$\alpha_{nf} = \frac{k_{eff}}{(\rho C_p)_{nf}} \tag{4}$$

$$\beta_{nf} = \varphi\rho_s\beta_s + (1-\varphi)\rho_f\beta_f \tag{5}$$

The effective density of the NF is given as [6]:

$$\rho_{nf} = (1-\varphi)\rho_f + \varphi\rho_s \tag{6}$$

The heat capacitance of the NF is expressed as [10]:

$$(\rho Cp)_{nf} = (1-\varphi)(\rho Cp)_f + \varphi(\rho Cp)_S \tag{7}$$

The dimensionless boundary conditions are written as:

$$\lambda = \frac{\dfrac{k_{nf}}{k_f}}{(1 - \varphi) + \varphi \dfrac{(\rho C p)_s}{(\rho C p)_f}} \qquad (14)$$

The dimensionless radial and tangential velocities are [20, 24]:

$$U = \frac{\partial \Psi}{\partial Y} \quad ; \quad V = -\frac{\partial \Psi}{\partial X} \qquad (15)$$

$$\lambda = \frac{\dfrac{k_{nf}}{k_f}}{(1 - \varphi) + \varphi \dfrac{(\rho C p)_s}{(\rho C p)_f}} \qquad (16)$$

Where the dimensionless numbers are [20, 24]:

$$Ra = \frac{g \beta H^3 (T_H - T_L)}{\upsilon \alpha} \qquad (17)$$

$$Pr = \upsilon / \alpha \qquad (18)$$

The Nusselt number can be expressed as:

$$Nu = \frac{hH}{k_f} \qquad (19)$$

The heat transfer coefficient is expressed as:

$$h = \frac{q_w}{T_H - T_L} \qquad (20)$$

The thermal conductivity is expressed as:

$$k_{nf} = -\frac{q_w}{\partial T / \partial x} \qquad (21)$$

Substituting Eqs (21), (20), and (8) into Eq. (19), and using the dimensionless quantities, the Nusselt number can be rewritten as:

$$Nu = -\left(\frac{k_{nf}}{k_f} \right) \frac{\partial \theta}{\partial X} \qquad (22)$$

The average Nusselt number along the hot wall surface can be obtained as:

$$Nu_m = \int_0^1 Nu(Y) dY \qquad (22)$$

Where

l: is the length of the hot wall.

On the left and right walls:

$$\theta = 0 \quad , \quad \psi = 0$$

On the top wall:

$$\theta = 0 \quad , \quad \psi = 0$$

On the bottom wall:

$$\theta = 1 \quad , \quad \psi = 0$$

Grid testing and cod validation

Based on ANSYS Fluent, the 2D conjugate heat transfer problem is numerically solved by a finite-volume approach using SIMPLE algorithm [29]. The algebraic system resulting from numerical discretization is solved by TDMA (Tridiagonal Matrix Algorithm) applied in a line going through all volumes in the computational domain. A non-uniform grid in x and y directions is used for all computations.

To test and assess the grid independence of the solution scheme, numerical experiments are performed as shown in Table 1. This study shows that an unequally spaced grid mesh of 80×120 is adequate to describe the flow, and heat transfer processes correctly. Also, the time running at $Ra = 10^5$ is 1284 second–mode coding in a computer with RAM 2.00 GB & CPU core(TM) i3 2.27 (4CPUs) GHz characteristics.

In order to substantiate the accuracy of the present computational code, the results of natural convection obtained from the present code are compared with the results of natural convection in a differentially heated square cavity (Fig. 2) [10, 19]. As seen in Fig. 2 the comparison of the present results for the Nusselt number showed excellent agreement with the two studies.

RESULTS AND DISCUSSIONS

In this research, heat transfer characteristics inside an inclined cavity filled with NF have been studied. We examined in this simulation the effects of the volume fraction (φ) of NP from 0% to 5%, the Rayleigh number from 10^3 to 10^6, the various inclination angles of enclosure (γ=0°,5°,10°, 15°) and the type of NF (Cu and Al₂O₃) on the flow streamlines, the isotherm distribution and the mean Nusselt number. The working NFs in the enclosure is chosen as Cu–water and Al₂O₃–water mixtures. The thermophysical properties of the base fluid (water) and NPs (Cu and Al₂O₃) are given in Table 2.

Table 1: Values of the stream function for different uniform grids.

Ra= 10^3				
Grid size	40×60	60×90	80×120	100×150
ψ_{max}	0.0345	0.0206	0.0276	0.0273

Table 2: Thermophysical properties of fluid and NPs.

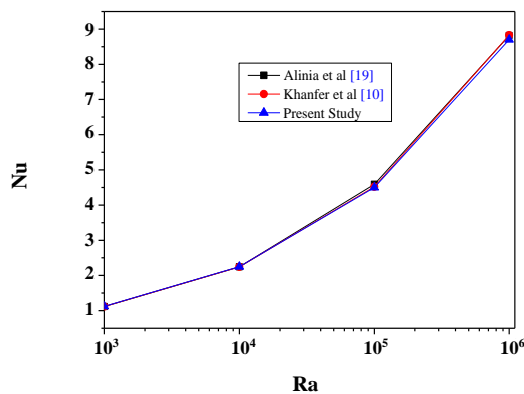| Physical properties	Fluid phase (water)	Cu	Al_2O_3
Cp (J/kgK)	4179	385	765
ρ (kg/m³)	997.1	8933	3970
k (W/mK)	0.613	400	40
$\alpha \times 10^7$ (m².s⁻¹)	1.47	1163.1	131.7
$\beta \times 10^5$ (1/K)	21	1.67	0.85

Fig. 2: Nusselt number and comparison with other published Works.

Figs. 3 and 4 show the streamlines and isotherms contours, respectively. Fig. 3 demonstrates that the streamlines are mostly symmetric. It is observed that by increasing the Rayleigh number, the stream function values generally increase, at low Ra numbers (Ra = 10^3 and 10^4) the value of the stream function is lowest and two secondary vortexes formed, contrariwise at high Ra numbers (Ra = 10^5 and 10^6) the vortexes stretched in the horizontal and vertical directions and their strength increases. Furthermore, we noted that the thickness of the thermal boundary layer next to the heated wall is sensitive to the presence of NPs and their volume fraction. The appearance of these two vortexes is due to the strong vorticity of the nanofluid particles near these regions.

The isotherms follow the geometry of the flat bottom flask (Fig. 4). This result is to be expected since under low

Rayleigh number conditions, a weak circulation structure formed, and thus minimal convection heat transfer occurs. However, under high Rayleigh number conditions (Ra = 10^6), the strength of the circulation structure within the cavity increases, and the heat transfer within the cavity is dominated by convection rather than conduction. In addition, it can be seen that the isothermal lines are concentrated near the bottom region of the hot wall and the left and right regions of the cold circular walls, which justifies the experiment made by Rayleigh-Bénard. Consequently, large temperature gradients are formed in the bottom region of the hot wall.

Figs. 5 and 6 represent the flow and thermal fields in terms of streamlines and isotherms contours, respectively, based on the four inclination angle of the cavity ($\gamma=0°,5°,10°, 15°$) for two types of NFs (Cu and Al_2O_3) with various volume fractions of NPs (φ =0.025, 0.05), at Ra = 10^5. The solid lines represent the results associated with the pure water ($\varphi = 0$), the dashed lines show the results pertaining to the Cu NPs and the dot-dashed lines show the Al_2O_3 NPs. Fig. 5 demonstrates that the streamlines are mostly symmetric. It is observed that increasing the inclination angle of the cavity, the value of the stream function generally decreases. By increasing volume fractions of NPs and therefore increasing the flow strength, streamlines become denser near the vertical wavy walls. At $\varphi = 0.05$, the form of vortexes is stretched in vertical and horizontal directions and are, for Cu, superior to Al_2O_3. Also, it is apparent from Fig. 6 that the isothermal lines are concentrated near the bottom region of the cavity and in the left and right regions of the cold circular walls.
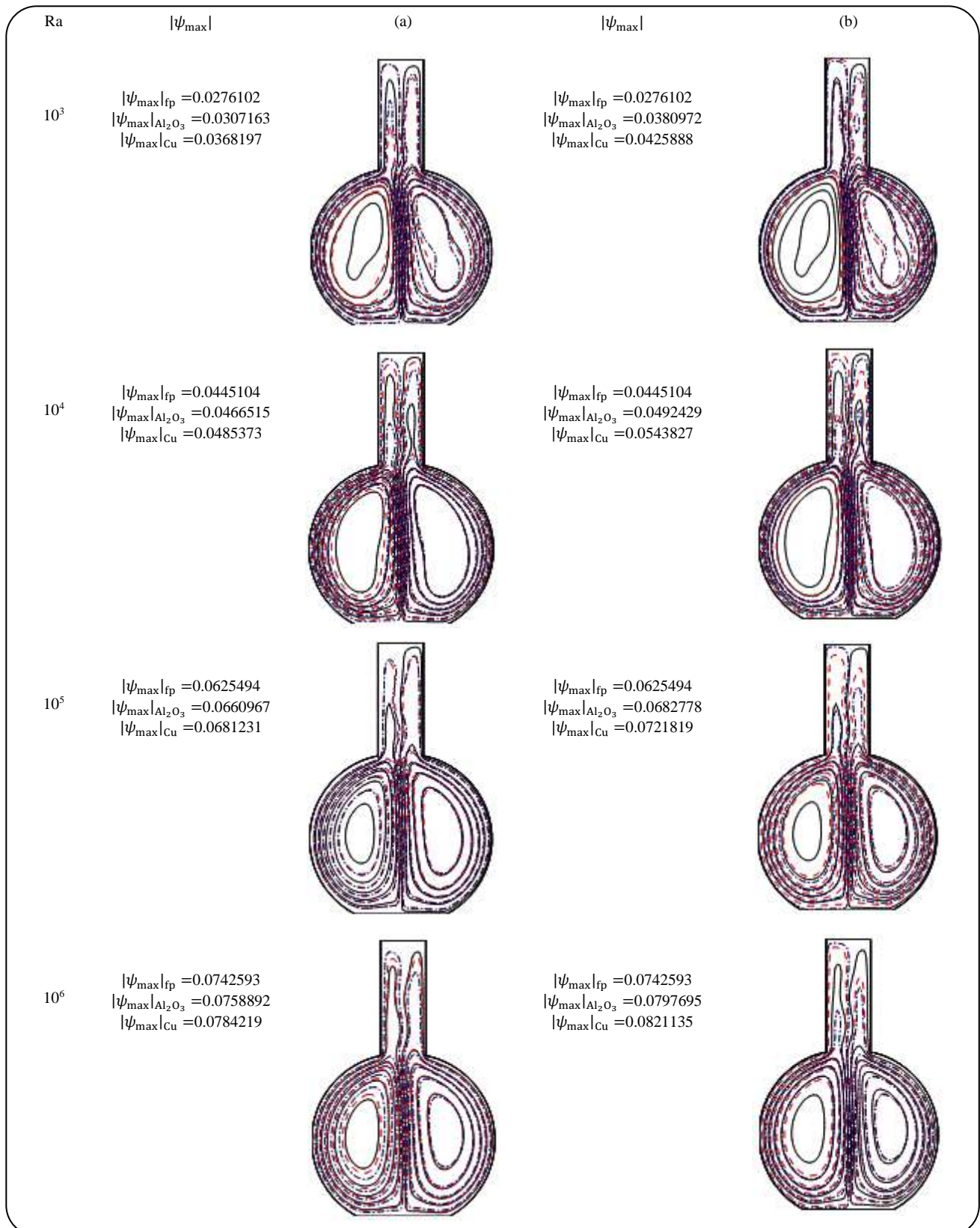
Ra	$|\psi_{max}|$	(a)	$|\psi_{max}|$	(b)
10^3	$|\psi_{max}|_{fp} = 0.0276102$ $|\psi_{max}|_{Al_2O_3} = 0.0307163$ $|\psi_{max}|_{Cu} = 0.0368197$		$|\psi_{max}|_{fp} = 0.0276102$ $|\psi_{max}|_{Al_2O_3} = 0.0380972$ $|\psi_{max}|_{Cu} = 0.0425888$	
10^4	$|\psi_{max}|_{fp} = 0.0445104$ $|\psi_{max}|_{Al_2O_3} = 0.0466515$ $|\psi_{max}|_{Cu} = 0.0485373$		$|\psi_{max}|_{fp} = 0.0445104$ $|\psi_{max}|_{Al_2O_3} = 0.0492429$ $|\psi_{max}|_{Cu} = 0.0543827$	
10^5	$|\psi_{max}|_{fp} = 0.0625494$ $|\psi_{max}|_{Al_2O_3} = 0.0660967$ $|\psi_{max}|_{Cu} = 0.0681231$		$|\psi_{max}|_{fp} = 0.0625494$ $|\psi_{max}|_{Al_2O_3} = 0.0682778$ $|\psi_{max}|_{Cu} = 0.0721819$	
10^6	$|\psi_{max}|_{fp} = 0.0742593$ $|\psi_{max}|_{Al_2O_3} = 0.0758892$ $|\psi_{max}|_{Cu} = 0.0784219$		$|\psi_{max}|_{fp} = 0.0742593$ $|\psi_{max}|_{Al_2O_3} = 0.0797695$ $|\psi_{max}|_{Cu} = 0.0821135$	

Fig. 3: Streamlines contours for various values of Rayleigh number, with (a) φ = 0.025, (b) φ = 0.05. For both the pure fluid (——) and NFs [(Cu (----) and Al₂O₃ (-.-.-)].
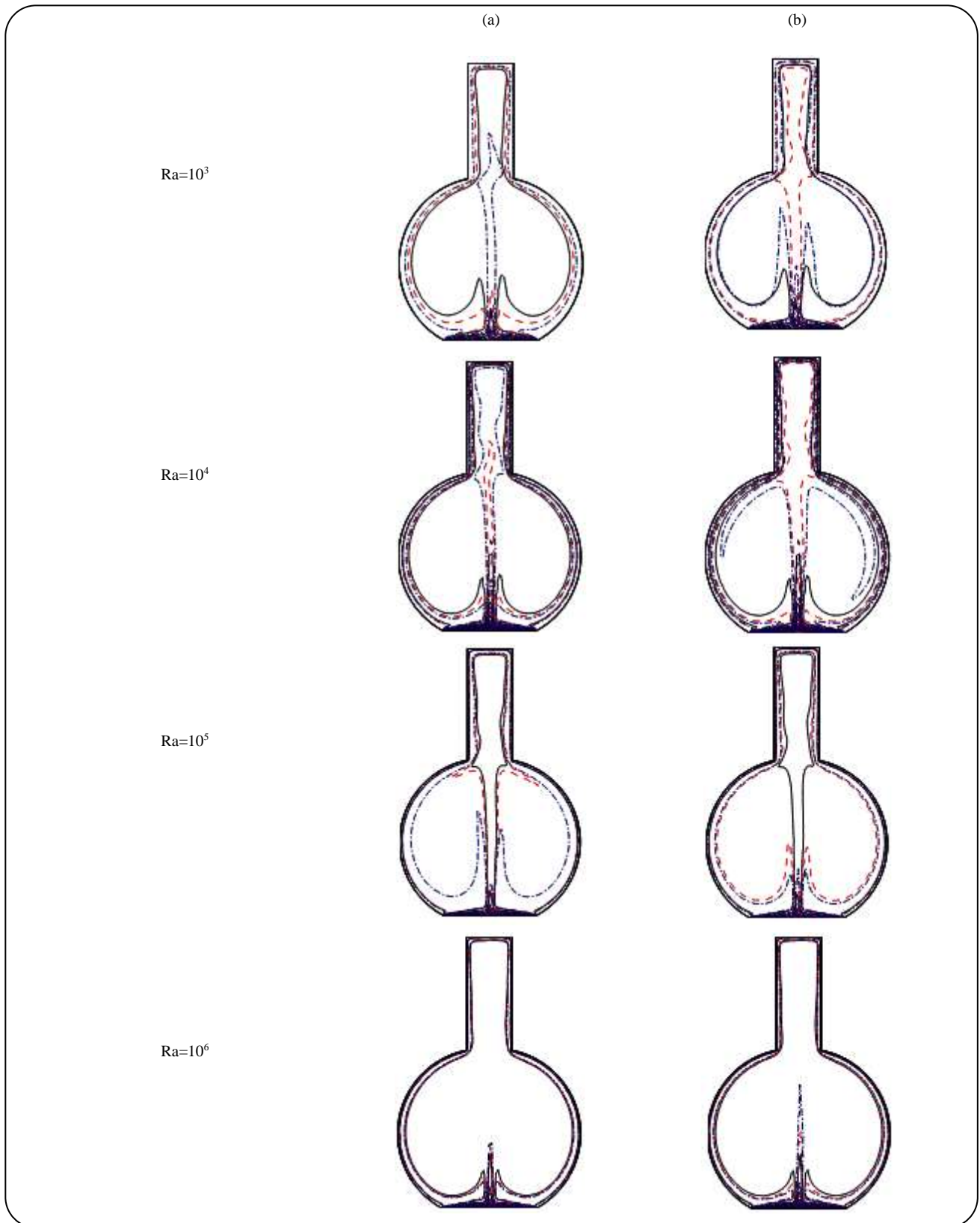
***Fig. 4: Isotherms contours for various values of Rayleigh number, with (a) φ = 0.025, (b) φ = 0.05. For both the pure fluid (—)
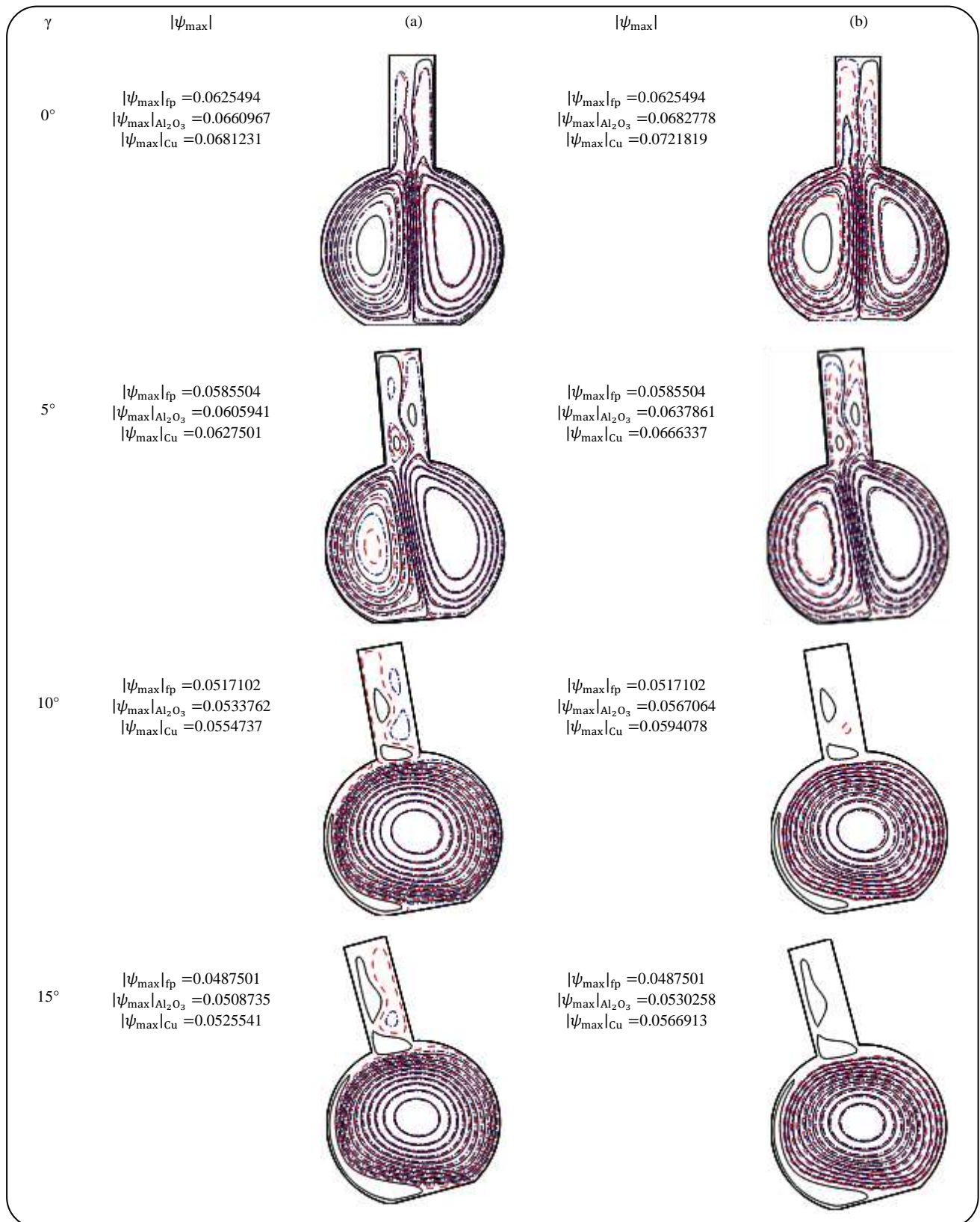and NFs [(Cu (----) and Al₂O₃ (-.-.-)].***

γ	$|\psi_{max}|$	(a)	$|\psi_{max}|$	(b)
0°	$|\psi_{max}|_{fp} = 0.0625494$ $|\psi_{max}|_{Al_2O_3} = 0.0660967$ $|\psi_{max}|_{Cu} = 0.0681231$		$|\psi_{max}|_{fp} = 0.0625494$ $|\psi_{max}|_{Al_2O_3} = 0.0682778$ $|\psi_{max}|_{Cu} = 0.0721819$	
5°	$|\psi_{max}|_{fp} = 0.0585504$ $|\psi_{max}|_{Al_2O_3} = 0.0605941$ $|\psi_{max}|_{Cu} = 0.0627501$		$|\psi_{max}|_{fp} = 0.0585504$ $|\psi_{max}|_{Al_2O_3} = 0.0637861$ $|\psi_{max}|_{Cu} = 0.0666337$	
10°	$|\psi_{max}|_{fp} = 0.0517102$ $|\psi_{max}|_{Al_2O_3} = 0.0533762$ $|\psi_{max}|_{Cu} = 0.0554737$		$|\psi_{max}|_{fp} = 0.0517102$ $|\psi_{max}|_{Al_2O_3} = 0.0567064$ $|\psi_{max}|_{Cu} = 0.0594078$	
15°	$|\psi_{max}|_{fp} = 0.0487501$ $|\psi_{max}|_{Al_2O_3} = 0.0508735$ $|\psi_{max}|_{Cu} = 0.0525541$		$|\psi_{max}|_{fp} = 0.0487501$ $|\psi_{max}|_{Al_2O_3} = 0.0530258$ $|\psi_{max}|_{Cu} = 0.0566913$	

Fig. 5: Streamlines at various inclination angles and various volume fractions of NPs: (a) φ = 0.025, (b) φ = 0.05. For both the pure fluid (—) and NFs [(Cu (----) and Al₂O₃ (-.-.-) and Ra = 10⁵.

Consequently, large temperature gradients are formed in the bottom region of the hot wall. Since the buoyancy effect becomes more intense as the volume fraction of NPs increases and the type of NF changes, the strength of the circulation structure within the cavity increases. As well, the increase of the volume fraction increases the values of the thermophysical properties of the nanofluids, in particular the thermal conductivity. This improves the heat transfer and consequently the isotherms are moved to the walls having low temperatures. The effect of the inclination angle on the isotherm lines is shown in Fig. 6. We can see that by decreasing the inclination angle, the natural convection effect is remarkable. As a result, the deviation of isotherms reduces and the isotherms become more stratified [19]. Therefore, it can be inferred that the heat transfer in the cavity is dominated by the conduction effect. This result is to be expected because, under the condition of a large inclination angle, a weak circulation structure is formed, so minimal convective heat transfer occurs [24]. Fig. 5 illustrates streamlines at various inclination angles for both the pure fluid and NFs. The streamlined distributions at initial inclination angle (γ=0°), show that there exist two large cells form separately, in the left and right regions of the cavity. Moreover, in the top corner of the cavity at γ=5°, there exists a relatively small cell. From γ=10°, the cavity is mainly occupied by a single large cell in the center of the cavity and a small cell in the left wavy wall. Also, the recirculation is anticlockwise and some perturbations are seen in streamlines which are characteristics of a cavity flow problem [19]. The numerical results indicate that good heat transfer was obtained for a vertical enclosure (γ=0°) and volume fractions of 0.05 where a good form of flow structure was observed.

Fig. 7 shows a diagram of the mean Nusselt number versus Rayleigh number for two different types of NFs (Cu and Al_2O_3) at an inclination angle ($\gamma = 0°$). As it is clear in this diagram, under this condition increasing Rayleigh number causes the mean Nusselt number and total heat transfer inside the cavity to increase. In addition, the type of NFs increases the mean Nusselt number and heat transfer inside the cavity. The maximum value of the mean Nusselt number was noted at Rayleigh 10^6 and for copper NPs.

Fig. 8 presents the variation of the mean Nusselt number with volume fraction using different NPs. The results are presented for Rayleigh number of 10^5 and inclination angle ($\gamma = 0°$).

The figure shows that the heat transfer increases with increasing the volume fraction for all NFs. It can be seen, that the lowest heat transfer was obtained for pure fluid due to the domination of the conduction mode of heat transfer because water has the lowest value of thermal conductivity compared to Cu and Al_2O_3. However, we observed a remarkable difference in the values of Al_2O_3 and Cu. As the volume fraction of NPs increases, the difference for the mean Nusselt number becomes larger especially at higher Rayleigh numbers due to increasing the domination of the heat transfer convection mode. The highest heat transfer is recorded when using Cu NP for $\varphi = 0.075$ and Ra = 10^5.

The change of mean Nusselt numbers versus different inclination angles is presented in Fig. 9 for a given Rayleigh number and volume fraction of NPs. Generally for all the types of NFs, as the inclination angle increases the mean Nusselt number decreases. For the horizontal cavity (γ= 0°), the mean Nusselt number has the highest value in comparison with other angles. This may be due to a single primary vortex throughout the cavity for the inclined cavities (from 10°). When the flat bottom wall of the cavity is horizontal or nearly horizontal, the presence of secondary vortices increases the Nusselt number. In conclusion, the highest heat transfer is recorded when using Cu NF for Ra=10^5, γ= 0°, and $\varphi = 0.05$.

CONCLUSIONS

The current study demonstrates the effects of the volume fraction (φ) of nanoparticles, the Rayleigh number, the various inclination angles of enclosure and the nanofluid type on the flow streamlines, the isotherm distribution, and the mean Nusselt number. Taken together, the main findings were:

1- The stream functions and Nusselt number increase by increasing Rayleigh number. In addition, it can be seen that heat transfer increases by increasing the Rayleigh number for a particular volume fraction.

2- Larger heat flow circulation cell occurs at the lowest inclination angles and the best heat transfer was obtained for a vertical enclosure (γ=0°).

3- The performance of Cu and Al_2O_3 nanofluids has been investigated, and they show better heating implementation as compared to pure water.

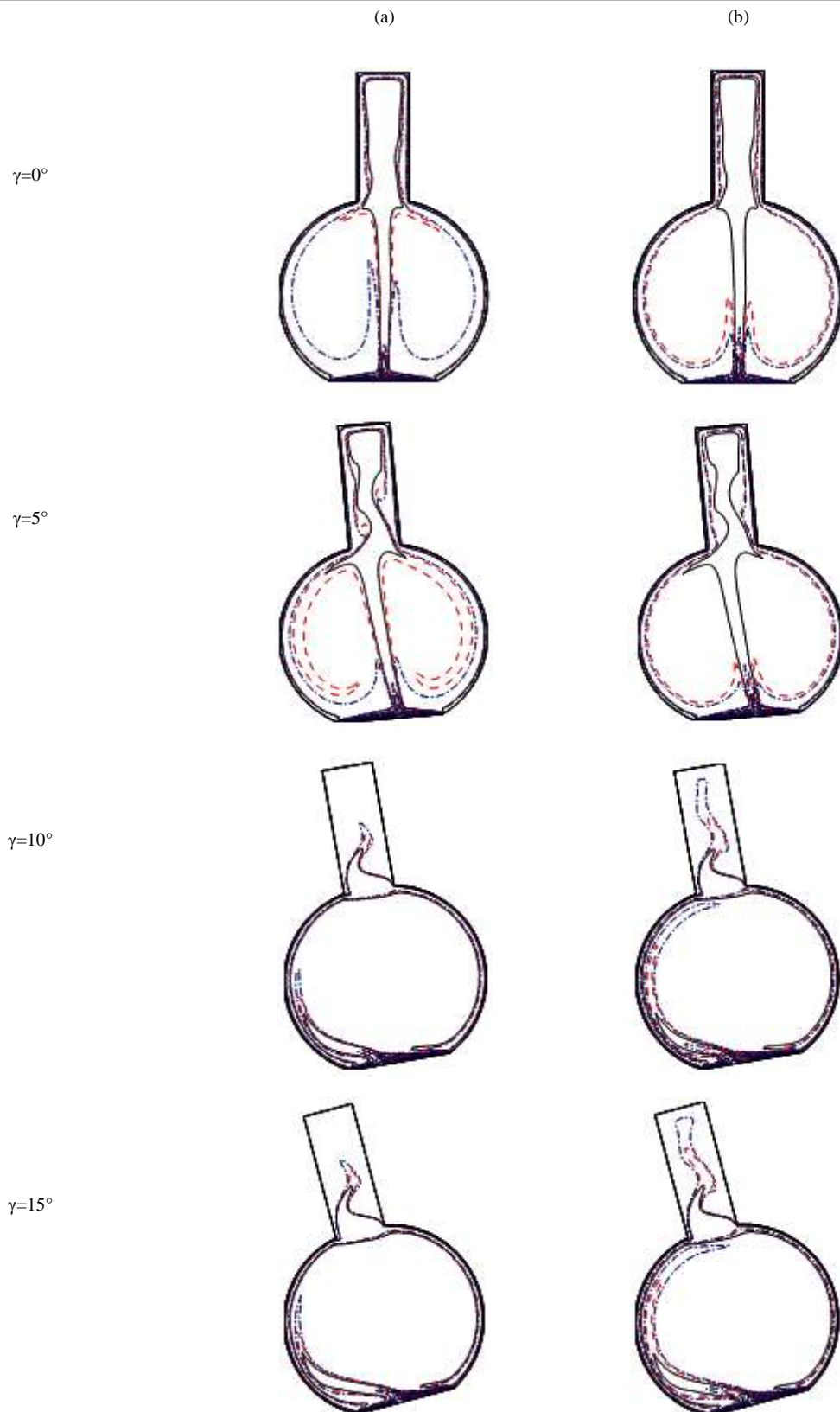4- The presence of Cu and Al_2O_3 nanoparticles results from an increase in Nusselt number.

Fig. 6: Isotherms at various inclination angles and various volume fractions of NPs: (a) φ = 0.025, (b) φ = 0.05. For both the pure fluid (—) and NFs [(Cu (----) and Al₂O₃ (-.-.-)] and Ra = 10⁵.

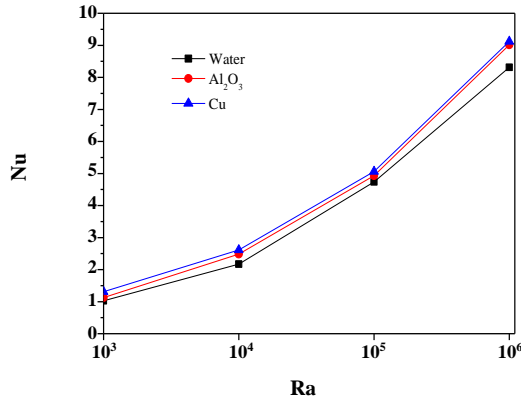*Fig. 7: Variation of mean Nusselt number with Rayleigh number as a function of NPs types. For both the pure fluid (φ = 0) and NFs (φ = 0.025) and at inclination angle γ = 0°.*
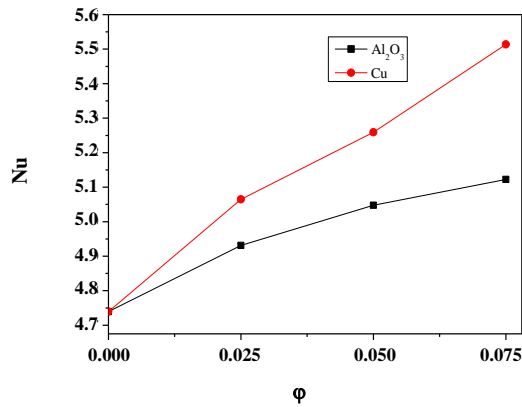

Fig. 8: Variation of mean Nusselt number with volume fraction of Cu and Al₂O₃ NPs. For Ra=10⁵ and γ = 0°.

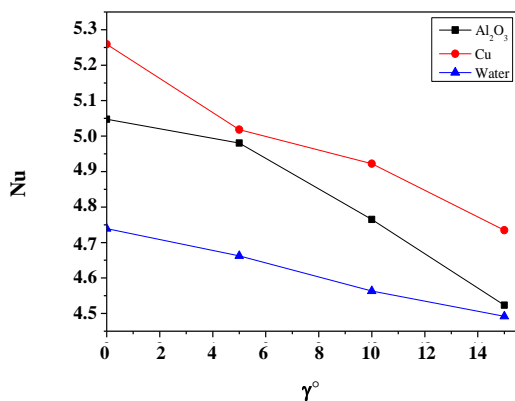*Fig. 9: Variation of mean Nusselt number with inclination angle as function of water, Cu and Al₂O₃ NPs. At Ra=10⁵ and φ = 0.05.*

5- For high Rayleigh numbers the difference in heat transfer increases by increasing the volume fraction value of nanoparticles.

6- The Cu–water nanofluid exhibits the best performance by providing the highest heat transfer.

Nomenclatures

C_p	Specific heat, J/kg.K
g	Gravitational acceleration, m/s²
T	Temperature, K
u, v	Components of velocity, m/s
U, V	Dimensionless components of velocity
x, y	Cartesian coordinates, m
X, Y	Dimensionless coordinates
H	Height of cavity, m
H	Heat transfer coefficient, W/(m².K)
q_w	Heat flux, W/m²
L	Height of the neck of the flask, m
D	Diameter of the flask, m
d_1	Diameter of the neck of the flask, m
d_2	Diameter of the bottom of the flask, m
l	length of the hot wall, m
k	Thermal conductivity, W/mK
Nu	Nusselt number
Pr	Prandtl number, $Pr = \upsilon_f / \alpha_f$
Ra	Rayleigh number, $Ra = g.\beta_f.\Delta T.H^3 / \upsilon_f / \alpha_f$
f	Fluid
s	Solide
nf or NF	Nanofluids
eff	Effective
NP	Nanoparticles
Cu	Copper nanoparticles
Al₂O₃	Alumina nanoparticles
MCHS	Microchannel heat sink
TDMA	Tridiagonal Matrix Algorithm

Greek symbols

α	Thermal diffusivity, m²/s
υ	Kinematic viscosity, m²/s
μ	Dynamic viscosity, N.s.m⁻²
ρ	Density, kg/m³
β	Thermal expansion coefficient, K⁻¹
Ω	Dimensionless vorticity
Ψ	Dimensionless stream function
θ	Dimensionless temperature

φ	Nanoparticle volume fraction
γ	Inclination angle

REFERENCES

[1] Choi S.U.S., Enhancing Thermal Conductivity of Fluids with Nanoparticles, *Dev. Appl. Non-Newtonian Flows*, **66**: 99–105 (1995).

[2] Motahari K., Barati S., Optimization of Nusselt Number of Al_2O_3/Water Nanofluid Using Response Surface Methodology, *Iran. J. Chem. Chem. Eng. (IJCCE)*, **38(3)**: 309-317 (2019).

[3] Yasuri A.K., Izadi M., Hatami H., Numerical Study of Natural Convection in a Square Enclosure Filled by Nanofluid with a Baffle in the Presence of Magnetic Field, *Iran. J. Chem. Chem. Eng. (IJCCE)*, **38(5)**: 209-220 (2019).

[4] Mohebbi K., Rafee R., Talebi F., Effects of Rib Shapes on Heat Transfer Characteristics of Turbulent Flow of Al_2O_3-Water Nanofluid inside Ribbed Tubes, *Iran. J. Chem. Chem. Eng. (IJCCE)*, **34(3)**: 61-77 (2015).

[5] Kargarsharifabad H., Experimental and Numerical Study of Natural Convection of Cu-Water Nanofluid in a Cubic Enclosure Under Constant and Alternating Magnetic Fields, *Int. Commun. Heat Mass Transfer*, **119(1)**: 104957 (2020).

[6] Hatami M., Zhou J., Geng J., Song D., Jing D., Optimization of a Lid-Driven T-Shaped Porous Cavity to Improve the Nanofluids Mixed Convection Heat Transfer, *J. Mol. Liq.*, **231(1)**: 620-631 (2017).

[7] Armaghani T., Kasaeipoor A., Alavi N., Rashidi M.M., Numerical Investigation of Water-Alumina Nanofluid Natural Convection Heat Transfer and Entropy Generation in a Baffled L-Shaped Cavity, *J. Mol. Liq.*, **223(1)**: 243-251 (2016).

[8] Ismael M.A., Armaghani T., Chamkha A.J., Conjugate Heat Transfer and Entropy Generation in a Cavity Filled with a Nanofluid-Saturated Porous Media and Heated by a Triangular Solid, *Journal of the Taiwan Institute of Chemical Engineers*, **59(1)**: 138-151 (2016).

[9] Aminossadati S.M., Ghasemi B., Natural Convection Cooling of a Localised Heat Source at the Bottom of a Nanofluid-Filled Enclosure, *Eur. J. Mech. B-Fluid*, **28(5)**: 630–640 (2009).

[10] Khanafer K., Vafai K., Lightstone M., Buoyancy Driven Heat Transfer Enhancement in a Two-Dimensional Enclosure Utilizing Nanofluids, *Int. J. Heat Mass Transfer*, **46(19)**: 3639–3653 (2003).

[11] Hwang K.S., Lee J.H., Jang S.P., Buoyancy-Driven Heat Transfer of Water-Based Al_2O_3 Nanofluids in a Rectangular Cavity, *Int. J. Heat Mass Transfer*, **50(19-20)**: 4003–4010 (2007).

[12] Hatami M., Song D., Jing D., Optimization of a Circular-Wavy Cavity Filled by Nanofluid Under the Natural Convection Heat Transfer Condition, *Int. J. Heat Mass Transfer*, **98(1)**: 758–767 (2016).

[13] Asadikia A., Mirjalily S.A.A., Nasirizadeh N., Kargarsharifabad H., Characterization of Thermal and Electrical Properties of Hybrid Nanofluids Prepared with Multi-Walled Carbon Nanotubes and Fe_2O_3 nanoparticles, *Int. Commun. Heat Mass Transfer*, **117(1)**: 104603 (2020).

[14] Talebi M., Kalantar V., Nazari M., Kargarsharifabad H., Experimental Investigation of the Forced Convective Heat Transfer of hybrid Cu/Fe_3O_4 Nanofluids, *Journal of Solid and Fluid Mechanics*, **8(4)**: 229-238 (2018).

[15] Asadikia A., Mirjalily S., Nasirizadeh N., Kargarsharifabad H., Hybrid Nanofluid Based on CuO Nanoparticles and Single-Walled Carbon Nanotubes: Optimization, Thermal, and Electrical Properties, *International Journal of Nano Dimension*, **11(3)**: 277-289 (2020).

[16] Hemmat Esfe M., Rostamian H., Influences of Temperature, Concentration and Shear Rate on Rheological Behavior of Nanofluid: An Experimental Study with Al_2O_3-MWCNT/10W40 Hybrid Nano-Lubricant, *Iran. J. Chem. Chem. Eng. (IJCCE)*, **38 (3)**: 319-328 (2019).

[17] Chamkha A., Armaghani T., Mansour M., Rashad A., Kargarsharifabad H., MHD Convection of an Al_2O_3–Cu/Water Hybrid Nanofluid in an Inclined Porous Cavity with Internal Heat Generation/Absorption, *Iran. J. Chem. Chem. Eng. (IJCCE)*, **41(3)**: 936-956 (2021).

[18] Saury D., Benkhelifa A., Penot F., Experimental Determination of First Bifurcations to Unsteady Natural Convection in a Differentially-Heated Cavity Tilted from 0° to 180°, *Exp. Therm Fluid Sci.*, **38**: 74–84 (2012).

[19] Alinia M., Ganji D.D., Gorji-Bandpy M., Numerical Study of Mixed Convection in an Inclined Two Sided Lid Driven Cavity Filled with Nanofluid Using Two-Phase Mixture Model, *Int. Commun. Heat Mass Transfer*, **38(10)**: 1428–1435 (2011).

[20] Tang W., Hatami M., Zhou J., Jing D., Natural Convection Heat Transfer in a Nanofluid-Filled Cavity with Double Sinusoidal Wavy Walls of Various Phase Deviations, *Int. J. Heat Mass Transfer*, **115** (Part A): 430–440 (2017).

[21] Ching-Chang C., Chieh-Li C., Cha'o-Kuang C., Natural Convection Heat Transfer Performance in Complex-Wavy-Wall Enclosed Cavity Filled with Nanofluid, *International Journal of Thermal Sciences*, **60(1):** 255–263 (2012).

[22] Ching-Chang C., Chieh-Li C., Cha'o-Kuang C., Natural Convection Heat Transfer and Entropy Generation in Wavy-Wall Enclosure Containing Water-Based Nanofluid, *Int. J. Heat Mass Transfer*, **61**: 749–758 (2013).

[23] Ching-Chang C., Ching-Huang C., Kuo-Ching C., Chong-You L., Natural Convection in Inclined Wavy-Wall Cavity Filled with Al_2O_3–Water Nanofluid Using Heatline Technique, *Journal of Mechanical Engineering and Automation*, **6(3)**: 65–70 (2016).

[24] Salhi H., Si-Ameur M., Haddad D., Numerical Study Of Natural Convection Heat Transfer Performance in an Inclined Cavity with Complex-Wavy-Wall: Nanofluid and Random Temperature, *Computational thermal sciences*, **7(1)**: 51–64 (2015).

[25] Kashani S., Ranjbar A.A., Mastiani M., Mirzaei H., Entropy Generation and Natural Convection of Nanoparticle-Water Mixture (Nanofluid) Near Water Density Inversion in an Enclosure with Various Patterns of Vertical Wavy Walls, *Applied Mathematics and Computation*, **226(1)**: 180–193 (2014).

[26] Sakanova A., Keian C.C., Zhao J., Performance Improvements of Micro Channel Heat Sink Using Wavy Channel and Nanofluids, *Int. J. Heat Mass Transfer*, **89**: 59–74 (2015).

[27] Ghasemi S.E., Hatami M., Solar Radiation Effects on MHD Stagnation Point Flow and Heat Transfer of a Nanofluid Over A Stretching Sheet, *Case Studies in Thermal Engineering*, **25(1)**: 100898 (2021).

[28] Brinkman H.C., The Viscosity of Concentrated Suspensions and Solutions, *J. Chem. Phys*, **20(4)**: 571–581(1952).

[29] Patnkar S.V., "Numerical Heat Transfer and Fluid Flow", Hemisphere Pub., New York (1980).